HiSST: 3rd International Conference on High-Speed Vehicle Science Technology
14 -19 April 2024, Busan, Korea

Development and Verification of Nonequilibrium Hypervelocity Reacting Flow Modeling in Open Source Framework

Kun Wu [1], Yu Ao [2], Yuting Jiang[3], Jianwen Liu[4], Xuejun Fan[5]

Abstract

Computational fluid dynamics (CFD) approach has become a crucial part of the design and study of modern high-speed space vehicles in recent years. In this work, a transient three-dimensional nonequilibrium CFD solver HiSCFOAM-NonE is developed in OpenFOAM to accomplish the computation of the hypervelocity reacting flows invovled in high Mach number scramjet engines. By coupling with the state-of-the-art thermal-chemical non-equilibrium package Mutation++, this solver is capable of simulating the chemical-reacting flow in scramjets operating in wide flight Mach numbers ranging from 8 to 15. The solver was primarily validated against a set of elementary benchmarks including zero-dimensional heat bath, high Mach number cylinder flow as well as complex shock-dominated flow in a model scramjet, wherein satisfactory agreements were obtained with the currently available experimental data.

[1] *Associate Professor, State Key Laboratory of High Temperature Gas Dynamics, Institute of Mechanics, Chinese Academy of Sciences, wukun@imech.ac.cn.*
[2] *Master Student, State Key Laboratory of High Temperature Gas Dynamics, Institute of Mechanics, Chinese Academy of Sciences.*
[3] *Engineer, Hefei Zhongke Chongming Technology Company.*
[4] *Senior Engineer, Beijing Power Machinery Institute.*
[5] *Professor, State Key Laboratory of High Temperature Gas Dynamics, Institute of Mechanics, Chinese Academy of Sciences.*

Keywords: High Mach number, thermal nonequilibrium, two-temperature model, chemical reaction, numerical simulation

Nomenclature

uppercase letters
Ma – Mach number
M_s – species molar weight
R_u – universal gas constant
T_{tr} – translational-rotational temperature
T_{ve} – vibrational-electronic temperature
Y_s – species mass fraction
lowercase letters
c_p^{tr} – translatinal-rotational specific heat capacity at constant pressure
c_p^{ve} – vibrational-electronic specific heat capacity at constant pressure
k_B – Boltzmann's constant
p – static pressure
x_s – species molar fraction
Greek
δ_{ij} – Kronecker delta
μ – dynamic viscosity
ρ – density
ρ_s – species partial density

1. Introduction

Computational fluid dynamic (CFD) approach has become a crucial part of the design and study of modern high-speed space vehicles in recent years. The complex flow fields surrounding these vehicles require the combination of different simulation tools. Particle-based direct simulation Monte Carlo (DSMC) [1] has been developed to solve for rarefied flows, which is characterized by the high Knudsen Number ($Kn > 0.05 \sim 0.1$). On the other hand, the conventional CFD simulations based on solving the Navier-Stokes equations remains capable when the Kn falls below 0.005 [2]. To extend the capability of the CFD approaches to solve hypersonic flows, more concerns should be taken to handle the effects of thermochemical nonequilibrium which is usually caused by the strong shock wave. Typically, thermochemical nonequilibrium effect becomes nonnegligible when the flow characteristic timescale is comparable to the thermal relaxation timescale and the chemistry characteristic timescale. In another word, the flow does not have enough time to reach the equilibrium state and the flow properties at these states would deviate a lot from that of the equilibrium state [3]. As a result, modeling these nonquilibrium effect in the continuum flow region is the key aspect of implementing the appropriate CFD simulation.

At high temperature, the total energy contained in the gas can be decomposed into different energy modes, namely the translational, rotational, vibrational and electronic modes. Each mode is designated to a corresponding temperature. Energy modes relax toward the thermal

equilibrium state via molecular collision. Generally, translational and rotational energies require very few collisions to reach equilibrium while for vibrational and electronic energies this number is much larger. As a result, it is reasonable to classify their corresponding temperatures into two groups, which forms the two-temperature model [3]. There have been some research codes that implemented this model, including the DPLR [4], LAURA [5], LeMANS [6, 7] and US3D [8, 9] . However, most of them are not open to public access. Other approaches can be found including the work made by Adhikari and Alexeenko [10] to implement the two-temperature model in Ansys Fluent, as well as the open-source nonequilibrium solver hy2Foam [11, 12] developed at the university of Strathclyde. Nevertheless, the work of Adhikari and Alexeenko is limited to the simulation of air flows while the implementation of hy2Foam is rather complicated which requires careful tuning of the model settings. The task of developing a robust solver which could deal with nonequilibrium hypervelocity flows especially for combustion with easy-to-use configrations is still needed.

Therefore, in the present work, a transient three-dimensional nonequilibrium CFD solver is developed to accomplish the computation of hypervelocity reacting flows invovled in high Mach scramjet engines. The theory of nonequilibrium reacting flows and the basic modules which form the base of this solver will be briefly described in the following. And primilary results including zero-dimensional heat bath, high Mach number cylinder flow as well as complex shock-dominated flow in a model scramjet will be present for numerical validation.

2. Governing equations and physical models

The nonequilibrium Navier-Stokes-Fourier equation in its conservative form is described as:

$$\frac{\partial \mathcal{U}}{\partial t} + \nabla \cdot (F^{inv} - F^{vis}) = \dot{\omega} \tag{1}$$

for the vector of conservative quantities

$$\mathcal{U} = (\rho, \rho_s, \rho u, \rho v, \rho w, E_{ve}, E)^T \tag{2}$$

where (u, v, w) is the velocity vector, E_{ve} and E are respectively the vibrational-electronic energy and the total energy. The total energy E is the combination of kinetic energy and the internal energy

$$E = \frac{1}{2}u^2 + \sum_{s \in S} Y_s e_s \tag{3}$$

in which S stands for the set of all species, and e_s is the specific internal energy which can be decomposed as

$$e_s = e_s^t + e_s^r + e_s^v + e_s^e + e_s^0 \tag{4}$$

Respectively, the translational, rotaional, vibrational, electronic and formation energy are given by

$$e_s^t = \frac{3}{2}\frac{R_u}{M_s}T_{tr} \tag{5}$$

$$e_s^r = \begin{cases} \frac{R_u}{M_s}T_{tr} & s\ is\ molecule \\ 0 & s\ is\ atom \end{cases} \tag{6}$$

$$e_s^v = \begin{cases} \frac{R_u}{M_s}\sum_v \frac{\theta_{v,s}^v}{\exp\left(\frac{\theta_{v,s}^v}{T_v}\right)-1} & s\ is\ molecule \\ 0 & s\ is\ atom \end{cases} \tag{7}$$

$$e_s^e = \frac{R_u}{M_s}\frac{\sum_i g_{i,s}\theta_{i,s}^e \exp\left(\frac{-\theta_{i,s}^e}{T_v}\right)}{\sum_i g_{i,s}\exp\left(\frac{-\theta_{i,s}^e}{T_v}\right)} \tag{8}$$

where $\theta_{v,s}^v$ is the characteristic vibrational temperature of species s and vibrational Special formatting mode v. $\theta_{i,s}^e$ is the characteristic electronic temperature of species s at energy level i and $g_{i,s}$ is the digeneracy temperature.

The inviscid flux F_i^{inv} is written as

$$F_i^{inv} = \begin{pmatrix} \rho u_i \\ \rho_s u_i \\ \rho u_i u + \delta_{i1}p \\ \rho u_i v + \delta_{i2}p \\ \rho u_i w + \delta_{i3}p \\ e_v u_i \\ (e_s + p)u_i \end{pmatrix} \quad for\ i = 1,2,3 \tag{9}$$

where p is calculated by the Dalton's law

$$p = \sum_{s \in S} p_s = \sum_{s \in S} (\rho_s R_u / M_s T_{tr}) \tag{10}$$

The viscous contribution to the flux is

$$F_i^{vis} = \begin{pmatrix} 0 \\ \mathcal{J}_{s,i} \\ \tau_{i1} \\ \tau_{i2} \\ \tau_{i3} \\ -q_{ve,i} \\ -\tau_{ij} u_j - q_{tr,i} - h_s \mathcal{J}_{s,i} \end{pmatrix} \quad for\ i = 1,2,3 \tag{11}$$

where τ_{ij} represents the viscous stress tensor

$$\tau_{ij} = \mu \left(\frac{\partial u_i}{\partial x_j} + \frac{\partial u_j}{\partial x_i} \right) - \frac{2}{3} \mu \frac{\partial u_i}{\partial x_j} \delta_{ij} \tag{12}$$

and $h_s = \int_{T_{ref}}^{T_{tr}} C_{p,s}^{Tr} dT$ denotes the enthalpy of species s. $C_{p,s}^{Tr}$ is the translational-rotational specific heat at constant pressure for species s.

The spatial heat conduction vector $q_{ve,i}$ and $q_{tr,i}$ can be calculated with the Fourier's law

$$q_{ve,i} = \alpha_{ve} \frac{\partial T_{ve}}{\partial x_i} \quad with\ \alpha_{ve} = \frac{\kappa_{ve}}{{c_p}^{ve}} \tag{13}$$

$$q_{tr,i} = \alpha_{tr} \frac{\partial T_{tr}}{\partial x_i} \quad with\ \alpha_{tr} = \frac{\kappa_{tr}}{{c_p}^{tr}} \tag{14}$$

Correspondingly, κ_{ve} and κ_{tr} are respectively the thermal diffusivity of the vibrational-electronic and translational-rotational energies.

The diffusion flux $\mathcal{J}_{s,i}$ is govened by the Fick's law:

$$\mathcal{J}_{s,i} = -\rho D_s \frac{\partial Y_s}{\partial x_i} \tag{15}$$

with the effective diffusive coefficient of species s

$$D_s = \frac{1 - x_s}{\sum_{j \neq s} x_j D_{sj}} \tag{16}$$

and D_{sj} is the binary diffusive coefficient [13]

$$D_{s,r} = \frac{k_B T_{tr}}{p \Delta_{tr}} \tag{17}$$

in which Δ_{tr} is the binary collision integral.

Finally, the source term $\dot{\omega}$, can be written as

$$\dot{\omega} = (0, \dot{\omega}_s, 0,0, 0, \dot{\omega}_{ve}, 0)^T \tag{18}$$

where the species source $\dot{\omega}_s$ is usually refered to the chemistry reactions

$$\dot{\omega}_s = M_{w,s} \sum_{r \in R} (v''_{sr} - v'_{sr}) \left[k_{f,r} \prod_{s \epsilon S} \rho_s^{v'_{sr}} - k_{b,r} \prod_{s \epsilon S} \rho_s^{v''_{sr}} \right] \Theta_r \tag{19}$$

where v'_{sr} and v''_{sr} is correspondingly the forward and backward reaction stoichiometry coefficient, ρ_s is the molar density, $k_{f,r}$ is the forward reaction rate and $k_{b,r}$ is the backward reaction rate. The forward reaction rate $k_{f,r}$ is determined by the modified Arrehenius' law and Park's coefficients [14]

$$k_{f,r}(T) = A T_c^n \exp\left(-\frac{T_a}{T_c}\right) \tag{20}$$

where A, n and T_a are correspondingly the reaction rate constant, the exponent coeffiecient and the activation temperature which are obtained from the experimental data. The controlling temperature T_c is determined by the following table.

Table 1. Controlling temperature depending on the type of reactions

Type of Reaction	Dissociation	Exchange
T_c	$\sqrt{T_{tr} T_{ve}}$	T_{tr}

The backward reaction rate $k_{b,r}$ can be calculated from

$$k_{b,r} = \frac{k_{f,r}}{K_c} \tag{21}$$

where K_c is the equilibrium constant determined by the Gibbs free energy.

The energy transfer source $\dot{\omega}_{ve}$ is the sum of the contrbution from the vibrational-transirotional energy relaxation and that from the the coupling between chemistry reactions and vibrational dissociation

$$\dot{\omega}_{ve} = \dot{\omega}_{V-T} + \dot{\omega}_{V-C} \tag{22}$$

where in $\dot{\omega}_{V-T}$ can be evaluated with Landau–Teller Equation [15] by assuming that the energy transfer among vibrational-electronic energy modes can be modeled as hamonic oscillator

$$\dot{\omega}_{V-T} = \sum_{s \in S} \rho_s \frac{e_s^v(T_{tr}) - e_s^v(T_{ve})}{\tau_m} \tag{23}$$

where τ_m is the molar-averaged relaxation time

$$\tau_m = \frac{\sum_{s \neq e} X_s}{\sum_{s \neq e} X_s / \tau_{m-s}} \tag{24}$$

which can be evaluated as the summation of Millikan- While emperical formular [16] and the Park's correction [14].

$$\begin{gathered} \tau_{m-s} = \tau_m^{MW} + \tau_m^P \text{ with} \\ \tau_m^{MW} = \frac{1}{p} \exp\left[A_{m,s}\left(T^{-\frac{1}{3}} - B_{m,s}\right) - 18.42\right] \\ \tau_m^P = \frac{1}{N_s \sigma_s \sqrt{\frac{8 R_u T_{tr}}{\pi M_s}}} \end{gathered} \tag{25}$$

where X_s is the molar fraction, N_s is the number density and σ_s is the effective cross section for vibrational relaxation.

$\dot{\omega}_{V-C}$ denotes the change of vibrational-electronic energy due to the construction or destruction of species, assuming a non-preferential dissociation model and given by

$$\dot{\omega}_{V-C} = \dot{\omega}_s e_s^v \tag{26}$$

3. Computational framework and numerical methods

To solve Eqs. (1) to (26), a finite-volume solver, named HiSCFOAM-NonE, is developed within the platform of OpenFOAM V7 [17, 18] which possesses a single temperature solver for high-speed compressible flows named rhoCentralFoam [19]. The rhoCentralFoam solver adoptes the central-upwind interpolation scheme of Kurganov et. al. [20] which is proved to be successful in non-reacting supersonic flow simulations, thus they are also inherited to the present hypersonic solver.

The closure of the governing equations requires an efficient method to calculated the thermodynamic, transport and chemical kinetic properties, as well as the source terms in Eqs. (19) and (22). This task is accomplished by linking the current solver to Mutation++ [21], an open-source library developed at the von Karman Institute for Fluid Dynamics. The basic code structure is schematizied in Fig. 1. During each time step, the fluid flow quantities, including the density ρ, the species mass fraction Y, the vibrational and internal energy (or temperature for t_0) are calculated by HiSCFOAM-NonE by solving Eq. (1), and provided to Mutation++ to evaluate the gas state. As a feedback, the thermochemical properties and associated source terms are transferred back for the closure of the governing equations.

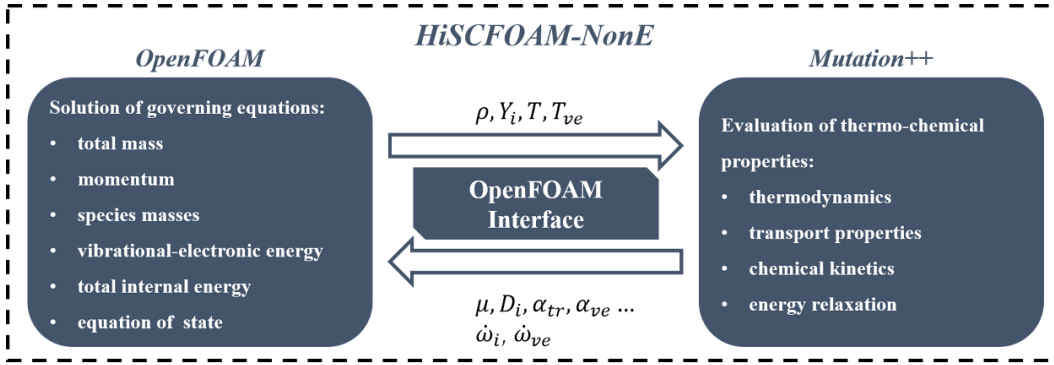

Fig 1. Diagram of the fracture of the HiSCFOAM-NonE solver showing the coupling between the OpenFOAM solver and Mutation++ library

4. Results and Discussion

Three computational baselines were conducted to assess the accuracy of the present solver. The first case considers the heat bath of nitrogen in thermal nonequilibrium. The vibrational heating (${T_v}^0 < {T_{tr}}^0$) and vibrational cooling (${T_v}^0 > {T_{tr}}^0$) cases are set according to the work of Boyd and Josyula [22]. The results of the solver are compared to the published data of LeMANS and MONACO [22] in Fig. 2. Excellent agreements are obtained with the present solver in comparison with the available published data.

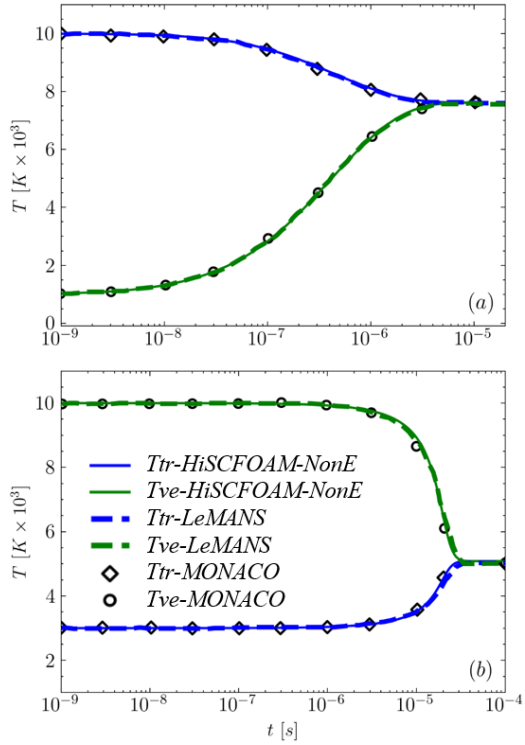

Fig 2. Relaxation of Vibrational and Translational Energy towards equilibrium of a $\boldsymbol{N_2}$ heat bath. (a) vibrational heating $\boldsymbol{{T_v}^0 = 1000\ K, {T_{tr}}^0 = 10000\ K}$ and $\boldsymbol{p^0 = 1\ atm}$; (b) vibrational cooling $\boldsymbol{{T_v}^0 = 10000\ K, {T_{tr}}^0 = 3000\ K}$ and $\boldsymbol{p^0 = 1\ atm}$.

Another two-dimensional simulation of reacting flow past a circular cylinder at Mach 8.78 [23] is performed for further validation. Following the experimental condition of Hannemann et. al.

[24]. The chemical mechanism [25] used and other simulation settings are illustrated in Table 2 and Table 3.The simulation was performed for two flow-through time.

Table 2. Gas mixture and mechanism [25]

No.	Reactions	Rate coefficients (A, n, T_a) $(\mathrm{cm \cdot mol^{-1} \cdot s^{-1}}, -, \mathrm{K})$	Third body efficiency (N2, O2, NO, N, O)
1	O2+M=2O+M	$(2.0 \times 10^{21}$, -1.5 , 59500)	(1.0, 1.0, 1.0, 5.0, 5.0)
2	N2+M=2N+M	$(7.0 \times 10^{21}$, -1.6, 113220)	(1.0, 1.0, 1.0, 4.286, 4.286)
3	NO+M=N+O+M	$(5.0 \times 10^{15}$, 0.0, 75500)	(1.0, 1.0, 1.0, 22.0, 22.0)
4	N2+O=NO+N	$(6.4 \times 10^{17}$, -1.0, 38400)	-
5	NO+O=O2+N	$(8.4 \times 10^{12}$, 0.0, 19450)	-

Table 3. Simulation condition of circular cylinder flow [24]

Inlet T_{tr} (K)	Inlet T_v (K)	Inlet U $(\mathrm{m \cdot s^{-1}})$	Inlet p (Pa)	Wall Temperature (K)	Inlet Mass fraction (N2, O2, NO, N, O)
694	694	(4776,0,0)	687	(300,300)	(0.736, 0.134, 0.051, $1x10^{-9}$,0.08)

The flow field calculated by HiSCFOAM-NonE is compared with that of another hypersonic nonequilibrium flow solver, named hy2Foam with the contour plots illustrated in Fig. 3. A good agreement of the flow field is obtained by the present solver in comparison with hy2Foam solver. Additionally, in Fig. 4(a), the density distributions along the stagation line obtained by these solvers are compared with the available data , both solvers captures the shock position with a little discrepency to the reference data. The comparison of pressure distribution along the cylinder wall is shown in Fig. 4(b), remarkable consistency is observed when comparing to the experimental data.

The last validation case considers the three-dimensional nonequilibrium flow in a model scamjet engine [26]. The structure of the engine is shown in Fig. 5. The computational mesh contains 694246 hexahedra grids.

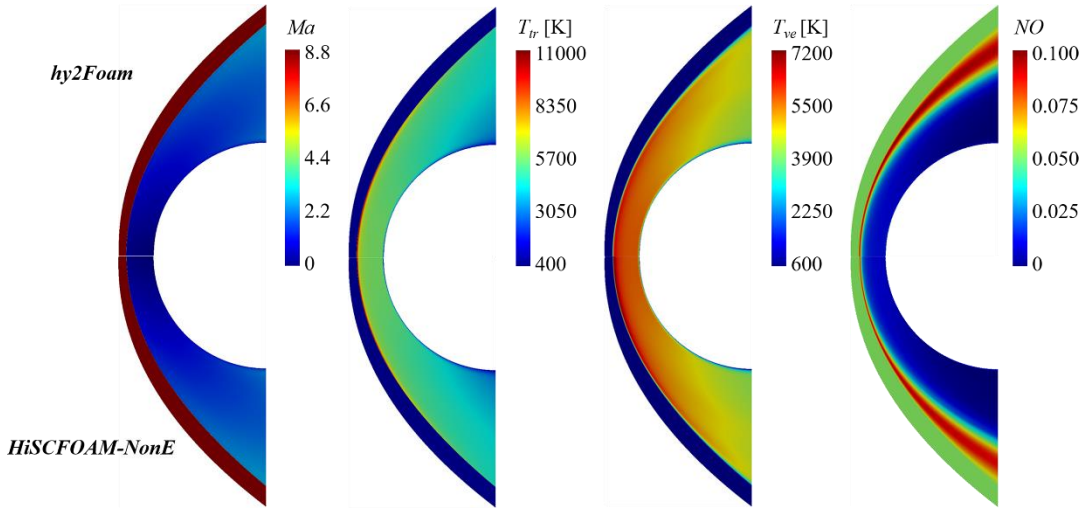

Fig 3. Comparison of contour plots of flow fields obtained with hy2Foam and HiSCFOAM-NonE for reacting flow past circular cylinder at Mach 8.78.

The simulation condition is listed in Table 4.

Table 4. Simulation conditions of the Lorrain scramjet engine [26]

Inlet T_{tr} [K]	**Inlet T_v [K]**	**Inlet U $[\mathrm{m \cdot s^{-1}}]$**	**Inlet p [Pa]**	**Wall Temperature (T_{tr}, T_{ve}) [K]**	**Inlet Mass Fractions (N2, O2, NO, N, O)**
260.68	640.32	(2734,0,0)	1877.99	(300,300)	(0.76, 0.223, 0.0168, 5.7×10^{-8},0.0)

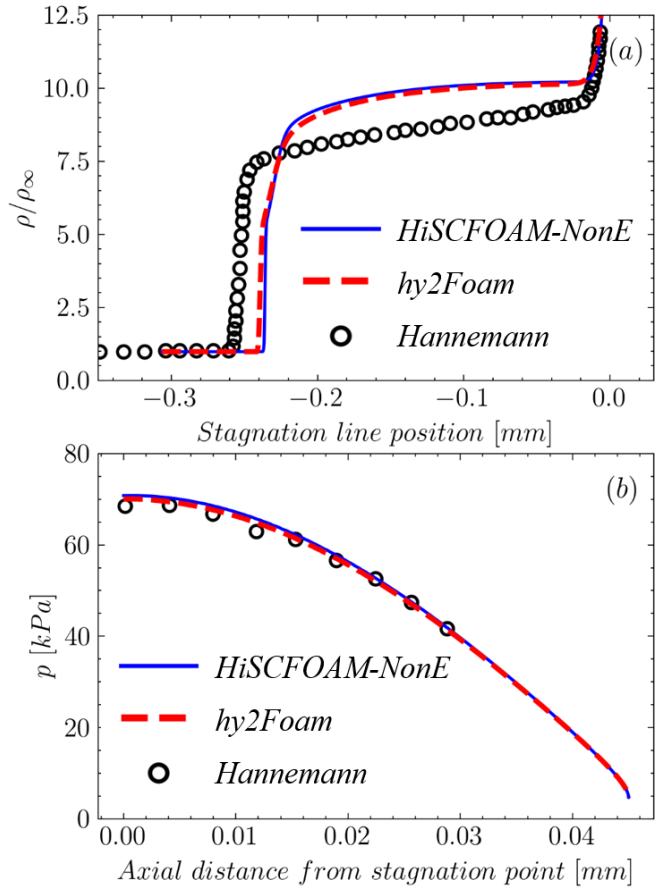

Fig 4. Comparison of (a) density along the stagnation line (b) pressure along cylinder wall obtained by HiSCFOAM-NonE and hy2Foam with the reference data obtained by Hannemann [24] for reacting flow past circular cylinder at Mach 8.78.

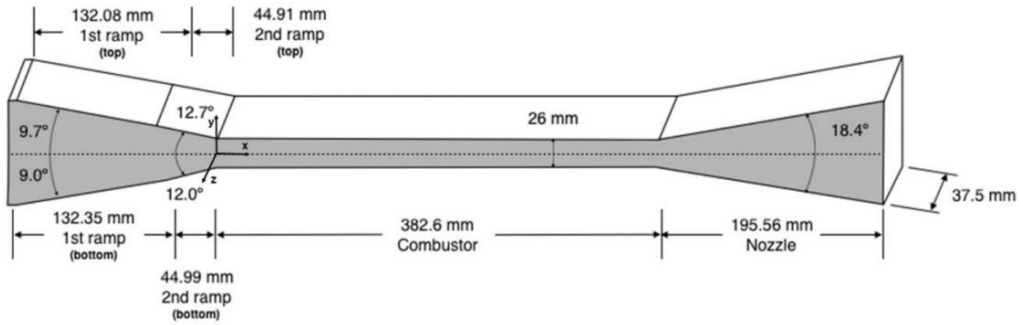

Fig 5. The model scramjet of Lorrain [26]

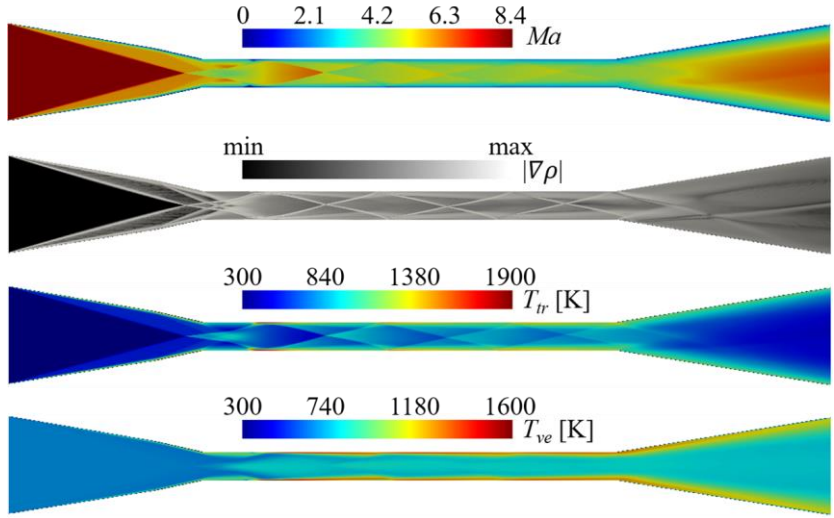

Fig 6. contour plots of flow fields obtained with HiSCFOAM-NonE in the Lorrain scramjet engine

A steady state simulation was adopted and the flow field is considered to become steady after executing the simulation for more than four flow-through time. The Reynolds-averaged SST model was employed to handle the turbulent influence. Fig. 6 illustrate the flow field contours obtained by HiSCFOAM-NonE.

It is clear that the sequence of shock waves is well-captured. The normalized pressure along the bottom wall obtained by HiSCFOAM-NonE and hy2Foam were compared with the experimental data as shown in Fig. 7. From the comparison, it is clear that HiSCFOAM-NonE captures the peak value of the normalized pressure (p/p_0) better than hy2Foam in this case.

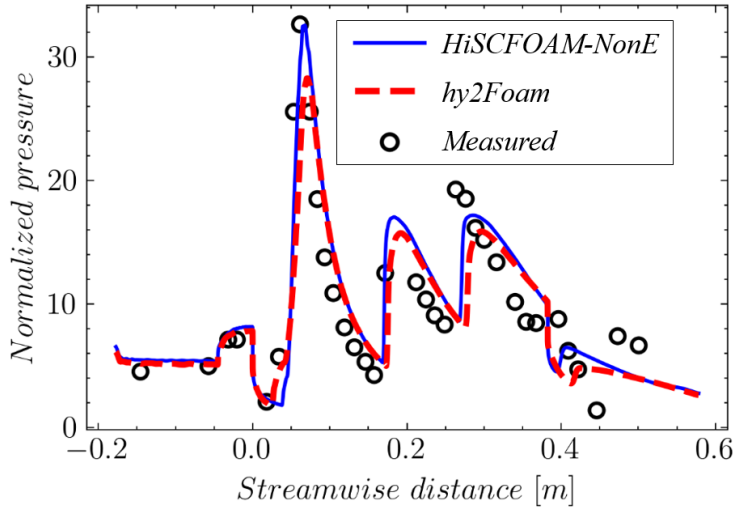

Fig 7. Comparison of the normalized pressure along the bottom wall obtained by HiSCFOAM-NonE and hy2Foam with the experimental data [26] for Lorrain scramjet engine.

5. Concluding remarks

In this work, a transient three-dimensional nonequilibrium CFD solver HiSCFOAM-NonE is developed in OpenFOAM to accomplish the computation of hypervelocity reacting flows involved in high Mach number scramjet engines. The solver was designed to broaden the capability of the CFD simulations by incorporating a two-temperature model which describes the nonequilibrium energy relaxation. It is capable of simulating thermo-chemical nonequilibrium flows in scramjets operating in wide flight Mach numbers ranging from 8 to 15. Compared to the currently available open-source solvers, this solver is more robust and efficient by virtue of the introduction of an open-source nonequilibrium thermodynamic package named Mutation++. The validity of this solver is evaluated by a set of elementary tests including zero-dimensional heat bath, high Mach number cylinder flow as well as complex shock-dominated

flow in a model scramjet. Results show satisfactory accuracy compared to the currently available experimental data.

References

1. Bird, G. A. "Molecular Gas Dynamics and the Direct Simulation of Gas Flows," *University of Oxford*, U.K, 1994
2. Hirschel, E. H. "Basics of Aerothermodynamics," *Springer*, Berlin, 2004
3. Park, C., "The Limits of Two-Temperature Kinetic Model in Air," 48th AIAA Aerospace Sciences Meeting Including the New Horizons Forum and Aerospace Exposition, Orlando, Florida, U.S.A, AIAA Paper 2010-357, January 2010
4. Candler, G. V., Wright, M. J., and McDonald, J. D. "Data-parallel lower-upper relaxation method for reacting flows," *AIAA Journal*, Vol. 32, No. 12, 1994, pp. 2380-2386
5. Cheatwood, F. M., and Gnoffo, P. A. "User's Manual for the Langley Aerothermodynamic Upwind Relaxation Algorithm (LAURA)," *NASA Technical Memorandum*, Washington, U.S.A, 1996
6. Scalabrin, L., and Boyd, I., "Development of an Unstructured Navier-Stokes Solver for Hypersonic Nonequilibrium Aerothermodynamics," 38th AIAA Thermophysics Conference, Toronto, Ontario, Canada, AIAA Paper 2005-5203, June 2005
7. Scalabrin, L., and Boyd, I., "Numerical Simulation of Weakly Ionized Hypersonic Flow for Reentry Configurations," 9th AIAA/ASME Joint Thermophysics and Heat Transfer Conference, AIAA Paper 2006-3773, June 2006
8. Nompelis, I., Drayna, T., and Candler, G., "Development of a Hybrid Unstructured Implicit Solver for the Simulation of Reacting Flows Over Complex Geometries," 34th AIAA Fluid Dynamics Conference and Exhibit, Portland, Oregon, U.S.A, AIAA Paper 2004-2227, June 2004
9. Candler, G. V., Johnson, H. B., Nompelis, I., Gidzak, V. M., Subbareddy, P. K., and Barnhardt, M., "Development of the US3D Code for Advanced Compressible and Reacting Flow Simulations," 53rd AIAA Aerospace Sciences Meeting, Kissimmee,

Florida, U.S.A, AIAA Paper 2015-1893, January 2015

10. Adhikari, N., and Alexeenko, A. "Development and Verification of Nonequilibrium Reacting Airflow Modeling in ANSYS Fluent," *Journal of Thermophysics and Heat Transfer*, Vol. 36, No. 1, 2021, pp. 1-11
11. Casseau, V., Espinoza, D., Scanlon, T., and Brown, R. "A Two-Temperature Open-Source CFD Model for Hypersonic Reacting Flows, Part Two: Multi-Dimensional Analysis," *Aerospace*, Vol. 3, No. 4, 2016, p. 45
12. Casseau, V., Palharini, R., Scanlon, T., and Brown, R. "A Two-Temperature Open-Source CFD Model for Hypersonic Reacting Flows, Part One: Zero-Dimensional Analysis," *Aerospace*, Vol. 3, No. 4, 2016
13. Alkandry, H., Boyd, I., and Martin, A., "Comparison of Models for Mixture Transport Properties for Numerical Simulations of Ablative Heat-Shields," 51st AIAA Aerospace Sciences Meeting, Grapevine (Dallas/Ft. Worth Region), Texas, U.S.A, AIAA Paper 2013-0303, January 2013
14. Park, C. "Review of chemical-kinetic problems of future NASA missions. I - Earth entries," *Journal of Thermophysics and Heat Transfer*, Vol. 7, No. 3, 1993, pp. 385-398
15. Schwartz, J. L., Abry, C., Boë, L. J., Vallée, N., and Ménard, L. "The dispersion-focalization theory of sound systems," *The Journal of the Acoustical Society of America*, Vol. 117, No. 4, 2005, pp. 2422-2422
16. Millikan, R. C., and White, D. R. "Systematics of Vibrational Relaxation," *The Journal of Chemical Physics*, Vol. 39, No. 12, 1963, pp. 3209-3213
17. Weller, H. G., Tabor, G., Jasak, H., and Fureby, C. "A Tensorial Approach to Computational Continuum Mechanics Using Object Orientated Techniques," *Computers in Physics*, Vol. 12, No. 6, 1998, pp. 620-631
18. Greenshields, and Christopher. "OpenFOAM v7 User Guide," *The OpenFOAM Foundation*, London, UK, 2019
19. Greenshields, C. J., Weller, H. G., Gasparini, L., and Reese, J. M. "Implementation of semi-discrete, non-staggered central schemes in a colocated, polyhedral, finite volume framework, for high-speed viscous flows," *International Journal for Numerical Methods in Fluids*, Vol. 63, No. 1, 2010, pp. 1-21

20. Kurganov, A., Noelle, S., and Petrova, G. "Semidiscrete Central-Upwind Schemes for Hyperbolic Conservation Laws and Hamilton--Jacobi Equations," *SIAM Journal on Scientific Computing*, Vol. 23, No. 3, 2001, pp. 707-740

21. Scoggins, J. B., Leroy, V., Bellas-Chatzigeorgis, G., Dias, B., and Magin, T. E. "Mutation + + : MUlticomponent Thermodynamic And Transport properties for IONized gases in C++," *SoftwareX*, Vol. 12, 2020, p. 100575

22. Boyd, I. D., and Josyula, E. "State resolved vibrational relaxation modeling for strongly nonequilibrium flows," *Physics of Fluids*, Vol. 23, No. 5, 2011, p. 057101

23. Guo, S.-Q., Liu, W., Zhang, C.-A., Zhou, X., and Wang, F.-M. "Simplified analytical models for hypersonic lateral-directional stability," *Acta Astronautica*, Vol. 198, 2022, pp. 431-444

24. Hannemann, K., Schramm, J. M., Karl, S., and Beck, W. H., "Cylinder Shock Layer Density Profiles Measured in High Enthalpy Flows in HEG," 22nd AIAA Aerodynamic Measurement Technology and Ground Testing Conference, St. Louis, Missouri, U.S.A, AIAA Paper 2002-2913, June 2002

25. Park, C. "Nonequilibrium hypersonic aerothermodynamics," *Wiley International*, New York, NY, U.S.A, 1990

26. Han, S., Lee, S., and Lee, B. J. "Numerical Analysis of Thermochemical Nonequilibrium Flows in a Model Scramjet Engine," *Energies*, Vol. 13, No. 3, 2020, p. 606